Selective hydrogenation of cinnamaldehyde by unsupported and few layer graphene supported platinum concave nanocubes exposing 110 facets stabilized by a long-chain amine

Laurent Peres, M. Rosa Axet, Deliang Yi, Philippe Serp, Aikaterini Soulantika

Selective hydrogenation of cinnamaldehyde by unsupported and few layer graphene supported platinum concave nanocubes exposing {110} facets stabilized by a long-chain amine

Laurent Peres,[a] M. Rosa Axet,[b] Deliang Yi,[a] Philippe Serp,[b]* Katerina Soulantica[a.]*

[a] *LPCNO, Université de Toulouse, CNRS, INSA, UPS, 135 avenue de Rangueil, 31077 Toulouse, France*

[b]*LCC-CNRS, Université de Toulouse, CNRS, INPT, Toulouse, France*

Abstract : Free and supported platinum concave nanocubes exposing {110} facets have been prepared by a wet-chemistry route and used as catalysts for the selective hydrogenation of cinnamaldehyde. The nanocubes were directly grown on few layer graphene support in the presence of octadecylamine as a stabilizing agent. Immobilization improves both activity and selectivity towards the desired unsaturated alcohol. The presence of organic stabilizers guarantees the stability of the nanoparticle morphology and influences the catalyst performances. While the activity is favored by small nanoparticles and low ligand contents, the selectivity to the unsaturated alcohol is favored by high ligand contents, most likely due to steric effects that favor adsorption through the C=O moiety. Apart from stabilizing the nanocubes, the support interacts with the long chain amine ligand, behaving as a ligand reservoir. Thus, an equilibrium established between the ligand interacting with the nanoparticles, the free ligand in solution, and the ligand interacting with the support redistributes the ligands during the catalytic reaction and assures a good compromise between activity and selectivity even after three recycling tests. While a direct comparison with other catalysts is not straightforward, the FLG-

supported concave nanocubes presented outstanding activity, and selectivity to cinnamyl alcohol higher than 80%.

1 Introduction

The development of sustainable heterogeneous catalysts demands the optimization of the catalyst activity, selectivity and stability. Since catalytic performances depend on the catalyst structural characteristics, a fine control over size, shape and composition is a priority target for optimization of the catalytic performances [1]. In this respect, the ongoing progress in nanocrystal synthesis by wet chemical routes offers the opportunity to elaborate optimized heterogeneous catalytic systems [2]. Thus, nanoparticles with tailored characteristics are being studied as catalysts in a large number of catalytic reactions [3]. Wet chemistry syntheses of nanocrystals make use of stabilizing agents (ligands) in order to control their size and direct their growth along certain crystallographic directions, thus determining their shape. Ligand influence on the performances of catalysts is very diverse. They can behave as poisons, blocking active sites or limiting the accessibility on the surface, or on the contrary as promoters, leading to improved yields and often unpredicted selectivity control, or even as simple spectators [4- 8].

Despite the advantages of their finely controlled structural characteristics, unsupported nanoparticles cannot be easily isolated and recycled [9]. Their immobilization on a macroscopic support enables easy recovery, catalyst recycling and improved stability through interactions with the support [10]. However, the conventional methods for the elaboration of supported catalysts do not allow a fine control of the nanoparticle size and shape [11]. Examples of immobilized, shape-controlled nanocrystals are thus less numerous [12-15]. Provided that the nanoparticle morphology and composition control achieved by solution approaches is reproducible on a support, the progress in nanocrystal synthesis could be of great benefit to

heterogeneous catalysis [16-18]. One of the problems associated to systems comprising colloidal nanoparticles is ligand removal, which often modifies the size and/or the shape of the particles. Thus, the advantages of morphologically tailored supported catalyst can be lost [4,6,7,19]. Alternatively, ligands presence on a supported catalyst can be exploited as it is the case for non-supported nanocatalysts. In order to benefit from the advantages that shape-controlled supported catalysts may offer, immobilization methods that allow shape-control of the catalytic phase should be developed.

The selective hydrogenation of compounds comprising various double bonds is an industrially relevant reaction, actively studied at the fundamental as well as at the applied level [20, 21]. Among such compounds, α,β-unsaturated aldehydes such as cinnamaldehyde (CAL) are excellent substrates for the evaluation of catalyst selectivity in the selective hydrogenation of C=C and C=O bonds. Platinum-based catalysts are intensively studied for this reaction. Nanoparticle size [22-24], composition [25, 26], shape [27, 28] and ligand coverage [29, 30] have been reported as decisive parameters in the cinnamaldehyde hydrogenation reaction, affecting both activity and selectivity. Contradictory results about the impact of nanoparticle size on activity have been reported [22, 23]. Recently, Durndell *et al*. showed that, while selectivity on Pt nanoparticles is very structure-sensitive, the activity is not [24]. Indeed, the calculations of Sautet and Delbeck on Pt and Pd surfaces, underline the better capacity of *cfc* {111} surfaces for promoting selectivity to the unsaturated alcohol cinnamyl alcohol, (COL) by favoring the coordination of the C=O instead of the C=C bond [31]. Bigger particles exposing extended {111} facets present less edges and vertices than small particles, affording better selectivity for the unsaturated alcohols [24]. Moreover, different types of surfaces can afford different activity and selectivity [12, 32, 33-35]. In most of these studies {111} and {100} thermodynamically stable surfaces have been compared, mainly due to the fact that the catalyst preparation methods employed do not allow metastable higher energy facets to be

stabilized. For example, for Pt/C catalysts, the catalytic performances showed a strong structure-sensitive character, with TOF following the trend Pt(100)/C > Pt(111)/C, and selectivity towards COL following the trend Pt(111)/C > Pt(100)/C [32]. Catalytic studies on shape-controlled supported Pt-containing nanocrystals either in thermal- or electro-catalysis mainly concern convex nanoparticles exposing the most stable {100} and {111} facets [12-14, 32, 36] and rare are the cases where more elaborated shapes have been employed on supports [15]. Recently, metal nanocrystals exposing high-index facets have drawn significant attention, mainly in electrocatalysis, due to their superior activity compared to that of low-index faces [15, 37-41]. The reactivity of high-energy facets has been much less investigated in thermal catalysis [42]. The comparison between concave (with exposed high-index facets) and standard cubes of bimetallic PtCo nanoparticles for CAL hydrogenation has proven the importance of nanoparticle shape and surface exposure, however the possible role of ligands has not been discussed [27]. The concave cubes (CCs) present better activity and selectivity towards COL in comparison with the standard cubes.

In this work we present the direct growth of concave nanocubes of platinum exposing {110} facets on few layer graphene (FLG), by adapting a wet chemistry method that produces free CCs in solution in the presence of octadecylamine. This has allowed the evaluation of both the unsupported and the FLG-supported CCs in the selective hydrogenation of cinnamaldehyde. The {110} facets of metals that crystallize in the *fcc* structure are low index, but they are composed of a high number of atoms of low coordination number, and as such they are expected to be more active [43]. Pt (110) model surfaces have been tested for the selective hydrogenation of prenal and it was found that at low prenal partial pressures C=C hydrogenation is favored, while higher prenal concentration promotes the selectivity to the unsaturated alcohol. This was attributed to the coverage dependent adsorption mode of the prenal [44]. These results were also supported by theoretical calculations [31]. Surprisingly,

pure Pt CCs exposing (110) type facets had not been available up to now despite the fact that bimetallic Pt-Sn CCs exposing {110} facets have been synthesized and studied in electrocatalysis [41]. The CCs discussed here are metastable objects, capped by stabilizing agents, which affect the catalytic performances. In this context, it is not the inherent reactivity of {110} facets that is evaluated, but the reactivity of {110} facets stabilized by octadecylamine. Here, we show that apart from the fact that ligands can stabilize the nanocrystal morphology under the conditions of the catalytic reaction, they can also promote high selectivity towards the most desired unsaturated alcohol without compromising the activity, which was found to be among the highest when compared to activities of Pt-based catalysts reported in the literature. The very high activity of this catalyst is most likely associated to the {110} facets.

2 Experimental section

2.1 Materials and methods

All syntheses were performed under inert conditions in order to avoid oxygen and water during the synthesis. After synthesis, the catalysts were handled under ambient conditions. $PtCl_2$ 98% and $PtCl_2$ 99.9% were obtained from Alfa Aesar. Octadecylamine (ODA - $C_{18}H_{39}N$, 98%) was purchased from Sigma-Aldrich. These products were introduced in a glovebox and used without any further purification. Toluene (99%) was purchased from VWR Prolabo, then purified on alumina desiccant and degassed through three freeze-pump-thaw cycles. Trans-cinnamaldehyde (99%), nonane (99%), isopropanol (99%), and pentane (99%) were obtained from Sigma Aldrich. 2-2-4-triméthylpentane (99%) was purchased from Acros Organics, degassed through three freeze-pump-thaw cycles and dried on molecular sieves.

Transmission electron microscopy (TEM) observations was carried out with a JEOL JEM 1400.

Catalytic hydrogenation reactions were carried out in a Top Industry stainless steel autoclave. Gas chromatography analyses were run on a Perkin Elmer Autosystem XL equipped with a Restek Rtx 5-Amine column (30 m, 0.53 mm, 1 μm).

The FLG support was synthesized by CVD following previous published procedure [45]. The Brunauer-Emmett-Teller (BET) analyses by N_2 adsorption isotherms at 77 K were performed on a QuantaChrome instrument. The thermogravimetric analysis (TGA) was performed with a TGA/DSC 1 Star System from Metler Toledo.

The ICP (Inductively Coupled Plasma) analysis was performed by Pascher (http://www.mikrolabor.com/).

2.2 Preparation of catalysts

2.2.1 CC-45

The unsupported concave cubes preparation followed a previous published procedure [46]. Briefly, the reactants, $PtCl_2$ 98% (16 mg, 6 10^{-2} mmol), ODA (400 mg, 1.5 mmol), and toluene (7 mL), were introduced in a Fischer Porter bottle in the glove box. After 10 min of homogenization of the mixture in an ultrasonic bath, the Fischer Porter bottle was charged with 3 bar of dihydrogen and then left at 20 °C for 168 h (one week) under magnetic stirring. At the end of the reaction, the bottle was depressurized and the final suspension was washed three times with a mixture of toluene and ethanol and centrifuged at 12 krpm for 10 minutes. Finally, 10 mL of pentane were added and, after decantation and supernatant removal, the nanoparticles were dried under vacuum.

2.2.2 CC-11.

The same procedure as for CC-45 was followed apart from the $PtCl_2$ 98% that was 7 mg; (2.6 10^{-2} mmol).

2.2.3 SCC-50

For the preparation of supported concave cubes over FLG, a Pt loading of 5% in mass with respect to the support was targeted. The reactants, $PtCl_2$ 98% (4 mg; 1.5 10^{-2} mmol), ODA (400 mg; 1.5 mmol), FLG (60 mg) and toluene (3.5 mL), were introduced in a Fischer Porter bottle inside the glove box. After 10 min of dispersion in an ultrasonic bath, the Fischer Porter bottle was charged with 3 bar of dihydrogen and then left at 25 °C for 168 h (one week) under magnetic stirring. At the end of the reaction, the bottle was depressurized and the final suspension was diluted by adding 10 mL of toluene, re-dispersed with the aid of ultrasound short treatment (1 min), and 10 mL of ethanol were added. The mixture was centrifuged at 10 rpm for 10 minutes. After removing the supernatant, 10 mL of toluene and 10 mL of ethanol were added. The operation was repeated three times. Finally, 10 mL of pentane were added and, after decantation and supernatant removal, the nanoparticles were dried under vacuum.

2.2.4 SCC-8

The same procedure as for the SCC-50 was followed, the only modification was the amount of $PtCl_2$ 98% (2 mg; 0.75 10^{-2} mmol)

2.2.5. NCC-6

The reactants, $PtCl_2$ 99.9% (16 mg, 6.10^{-2} mmol), ODA (400 mg, 1.5 mmol), and 2-2-4-triméthylpentane (7 mL), were introduced in a Fischer Porter bottle in the glove box. After 10 min of homogenization of the mixture in an ultrasonic bath, the Fischer Porter bottle was charged with 3 bar of dihydrogen and then left at 100 °C for 24 h under agitation. At the end of the reaction, the bottle was depressurized and the final suspension was washed three times with a mixture of toluene (7 mL) and ethanol (15 mL) and centrifuged at 20 krpm for 10 minutes. Finally, 7 mL of pentane and 15 mL of ethanol were added and, after decantation and supernatant removal, the nanoparticles were dried under vacuum.

2.3 Catalyst characterization

The catalysts have been observed by transmission electron microscopy (TEM) before and after the catalytic runs. The Pt content in all catalysts has been determined by ICP. The ligand content in the supported catalysts was determined by TGA analysis, and corresponds to the first loss of mass observed between 200 °C and 250 °C.

In Table 1 we present the size of the Pt nanoparticles of each catalyst and their content in ligands and metal.

Catalyst	Size (nm)	% Ligand	% Pt
CC-11	11.5 ± 4.8	4.7	95.3
CC-45	45.1 ± 7.7	13.3	86.7
NNC-6	6.1±0.7	12.1	87.9
SCC-8	7.8 ± 3.0	2.9	5.8
SCC-50	50.2 ± 13.8	3.0	5.0

2.4 Catalytic tests

The ICP analysis of the FLG support prior to Pt growth has shown that the FLG contained residual iron and cobalt from the catalyst used for its synthesis, Co = 0.05% and Fe = 0.09%. These metals are not accessible, and blank experiments for the hydrogenation of cinnamaldehyde have shown no activity of the FLG for this reaction.

Catalyst amounts corresponding to about 10 mg (9 ± 1 mg) of Pt were precisely weighted and inserted in the autoclave. A solution of trans-cinnamaldehyde (1 g) and nonane (0.47 g) in isopropanol (50 mL) prepared in the glove-box was introduced into the autoclave. The autoclave was purged three times with 3 bar of N_2 and three times with 5 bar of H_2. Then the autoclave was pressurized with 20 bar of H_2 and heated to 70 °C under stirring (1000 rpm). Samples of the reaction mixture were taken periodically and then analysed by GC. After the desired reaction time, the autoclave was cooled to room temperature and depressurised. The reaction mixture was then analysed by gas chromatography. Quantitative analyses of the

reaction mixtures were performed *via* GC techniques using calibration solutions of commercially available products.

A pre-reduction step was investigated in some cases. For that, the same procedure as above was followed, however, the amount of solvent was 40 mL and no cinnamaldehyde was introduced in the autoclave. After the pre-reduction step, that lasted 4 hours, the autoclave was depressurised and a TEM sample was obtained in order to verify the evolution of the morphology of the nanocrystals. Then a solution prepared in the glovebox containing the cinnamaldehyde (1 g) and nonane (0.47 g) in isopropanol (10 mL) was transferred to the reactor. The autoclave was pressurized with 20 bar of H_2 and heated to 70 °C under stirring (1000 rpm) for different reaction times. After the desired reaction time, the autoclave was cooled to room temperature and depressurised. The reaction mixture was then analysed by gas chromatography. For the recycling experiments, the catalyst was recovered by centrifugation and washed twice with pentane (10 mL). After drying, the catalyst was introduced into the glovebox and weighted before being re-used. The %Pt in the catalyst was considered constant during all the recycling experiments.

3. Results and discussion

Platinum concave nanocubes of two different sizes CC-11 and CC-45 (11.5 ± 4.8 nm and 45.1 ± 7.7 nm, respectively) exposing {110} type facets have been synthesized at room temperature by reduction under H_2 of $PtCl_2$ in the presence of octadecylamine (ODA) as stabilizing ligand (molar ratio Pt/ODA = 1/24.7) [46]. In Fig. 1a-b we present TEM images of the two as-prepared CCs. They were tested in the selective hydrogenation of cinnamaldehyde (Fig. 1c) at 70 °C under 20 bar of H_2. Hydrogenation of the C=O group leads to cinnamyl alcohol (COL), while hydrogenation of the C=C group forms hydrocinnamaldehyde (HCAL). Further hydrogenation of either COL or HCAL leads to the formation of hydrocinnamyl alcohol (HCOL). Other

reactions such as aromatic ring hydrogenation or hydrogenolysis are possible, but these generally require harsher conditions than the ones used in this study. The catalytic performances have been evaluated at 1 h and at 24 h reaction time, and the results plotted as bar diagrams in Fig. 1d-e for the CC-11 and CC-45, respectively. The schematic representation of the products in Fig. 1c serves as a guide for the catalysis results in Fig. 1d-e. The evolution of the catalyst morphology has been examined by TEM observations of the samples after 24 h of reaction (Fig. 1f-g for the CC-11 and CC-45, respectively). The results for all catalysts together with their Pt/L ratios (L= stabilizing ligands) are given in Table 2. Apart from their difference in size the two catalysts differ in the amount of stabilizing ligands on their surface. Indeed, CC-45, in addition to exposing a smaller total surface area due to their larger size, are stabilized by a higher amount of ligands. A simple purification protocol of the nanocrystals (see experimental section) removes the stabilizing ligands only partially, and to a different degree for each catalyst. This difference has to be considered for the interpretation of the catalytic results, since the presence of ligands may impact both activity and selectivity. The activity is very often negatively impacted by the ligands due to the reduction of the catalyst surface accessibility. Additionally, the presence of ligands prevents an evaluation of the number of active sites. Thus, catalyst activity can only be calculated over the total amount of Pt of each system. As far as selectivity is concerned, several reports have shown that the presence of ligands on the nanoparticle surface can significantly impact the selectivity in CAL hydrogenation both in unsupported but also supported nanocrystals [29, 30, 47, 48].

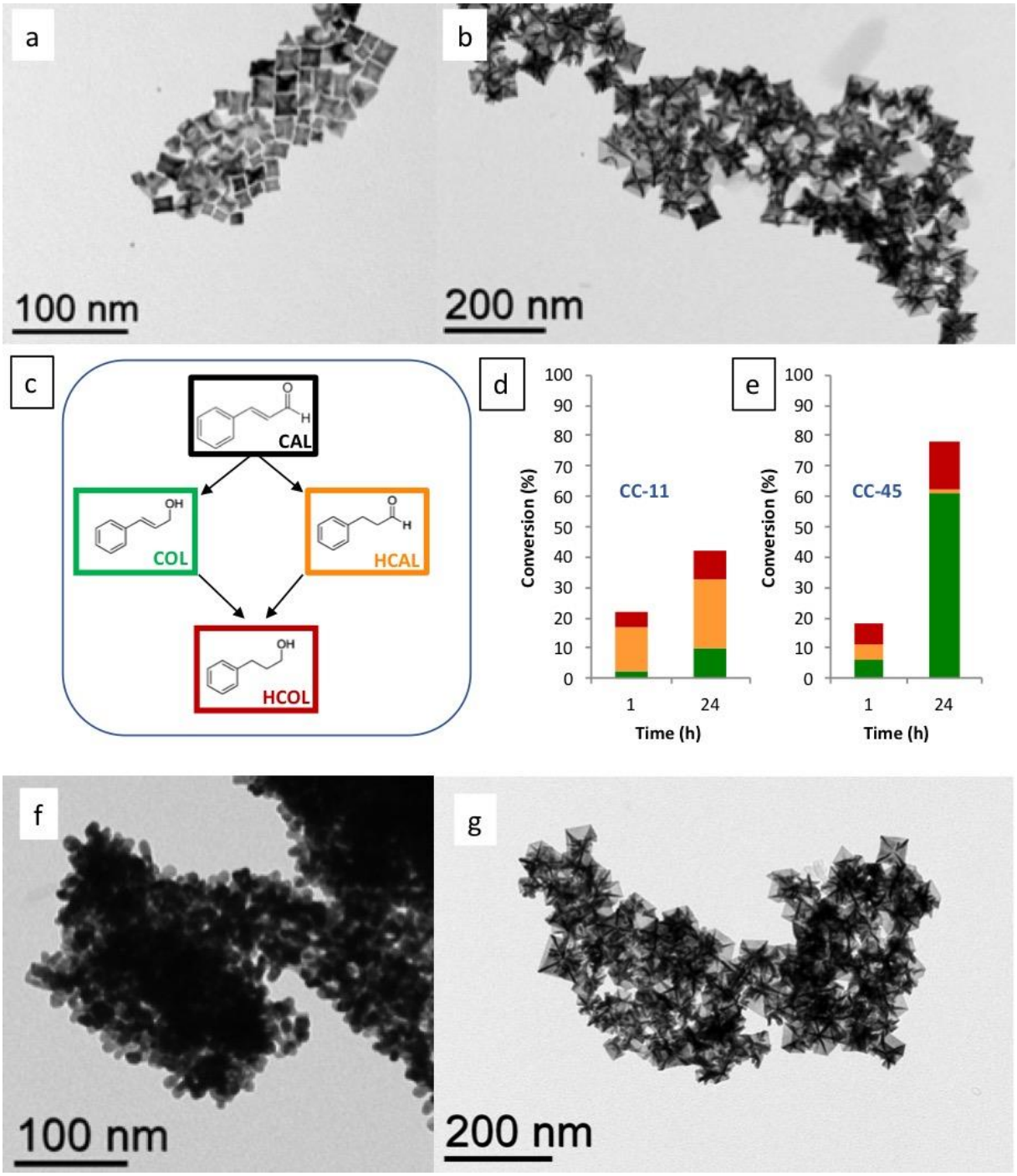

Fig. 1. Non-supported Pt CCs. TEM images of the as-prepared (a) CC-11; (b) CC-45; (c) reactant and products of the catalytic reactions; catalytic results for (d) the CC-11 and (e) the CC-45; TEM after 24h reaction of (f) the CC-11 and (g) CC-45.

Considering size as well as surface coverage by the ligands, the 11 nm CCs should present higher activity. This is true at 1 h of reaction. However, after 24 h, the activity of CC-45 is

higher than the one of CC-11 (9 and 3 h^{-1}, respectively). Comparison of the TEM micrographs of the catalysts before and after catalysis shows that the smaller CCs are severely impacted by the hydrogenation reaction. Indeed, the concavity of the CC-11 has been lost, and large aggregates of ill-shaped particles have been formed. The severe aggregation of CC-11 can explain the reduced conversion at 24 h. On the other hand, the CC-45 seem to have resisted and only marginal shape alterations can be detected, however aggregation has also been observed for this sample after catalysis, although to a less extent than in the case of CC-11. The shape conservation of CC-45 during catalysis could be result from the better stability of the bigger size and/or to the presence of more ligands.

As far as selectivity is concerned, the CC-11 catalyst presents a better selectivity towards HCAL, which is what is expected from the thermodynamically favored C=C hydrogenation versus C=O hydrogenation, and from the fact that smaller nanocrystals with high number of undercoordinated atoms allow easy approach of the C=C bond [24, 49]. Similar selectivity was reported for aggregated Pt nanoparticles of ill-defined shape stabilized by oleic acid ligands [47]. As the CC-11 catalyst is not stable under the reaction conditions, we cannot evaluate the influence of the type of facet exposed on the catalyst performances. The higher selectivity to COL of the CC-45 catalyst could be associated to various parameters, such as the ligand coverage, the type of facets exposed, or the particle size. Indeed, the CC-45 catalyst presents a high coverage by ligands (Pt/L = 6.5 % w/w), which allow an easier access to the Pt of the less sterically demanding C=O moiety compared to the C=C. Long-chain amine ligands have been reported to improve the selectivity for COL thanks to this steric effect [29]. Steric effects could also account for the increase of the COL selectivity with time on both catalysts, which is however, less pronounced for CC-11. This phenomenon has been observed before, and has been attributed to the gradual adsorption of intermediates on the catalyst surface, which favor the approach and subsequent hydrogenation of the less sterically demanding C=O bond [24,25].

The higher selectivity of CC-45 could also arise from the type of facets exposed. Indeed, as the CC-45 catalyst shape is not significantly modified during catalysis, we can envisage also an influence of the type of facets exposed on catalyst performances. To check this hypothesis, we independently prepared non-concave Pt nanocubes NCC-6 (size 6.1 ± 0.7 nm, ratio Pt/L = 7.3) exposing {100} facets, which have been reported as slightly less selective than the {111} facets [32]. The TEM micrographs of NCC-6 before and after catalysis as well as the graphs of the catalysis results are presented in Fig. S1 (Supplementary Material). It can be seen, that while aggregation after catalysis is observed for NCC-6, their shape is slightly rounded at the corners thus, much less modified as compared to the CC-11 nanocrystals of similar size. This is not surprising since these nanocubes are enclosed by more stable {100} facets. The NCC-6 sample, presents a similar Pt/L ratio as CC-45, but smaller particle size. The results on its catalytic performances are also presented in Table 2 (entry 4). Although this catalyst shows a similar Pt/L ratio as the CC-45 catalyst, NCC-6 activity is very low and its selectivity towards COL is also lower, for both reaction times. But it is also known that COL selectivity is significantly affected by Pt particle size [24], larger particles allowing higher selectivity. At this stage, it is difficult to de-correlate all these effects and attribute the performance to the size, shape or, ligand content. However, taking into account the results of Pradier *et al*. [44] in the case of prenal hydrogenation on Pt(100) model catalysts, who show that the selectivity of Pt(100) to the unsaturated alcohol was only favored by increasing the prenal partial pressure (steric effects), it is very likely that ligand coverage plays a major role on selectivity. For the most interesting non-supported catalyst CC-45 tested, the conversion and the selectivity towards COL at 24 h both reach at 78%.

Table 2. Catalyst performances of the unsupported and supported Pt concave nanocubes.

Exp.	Catalyst	Pt/L (w/w)	t (h)	conversion (%)	Activity (h^{-1})	selectivity (%)		
						COL	HCAL	HCOL
(1)	CC-11	20.3	1	22	37	11	64	25
			24	42	3.0	23	55	22
(2)	CC-45	6.5	1	18	25	33	29	38
			4	26	9	60	6	34
			24	78	5	78	2	20
(3)[a]	CC-45-H_2	6.5	1	18	28	71	9	20
			4	44	17	79	4	17
			24	79	5	83	1	16
(4)	NCC-6	7.3	1	13	24	6	65	29
			24	19	2	37	45	18
(5)	SCC-8 nm	2.0	1	58	91	43	35	22
			24	99	6	26	0	74
(6)	SCC-50	1.7	1	37	70	38	40	22
			4	54	25	45	32	23
			24	83	6	53	17	30
(7)[b]	SCC-50-H_2	1.7	1	54	209	83	5	12
			4	85	83	82	2	16
			24	93	15	67	1	32
Recycling 1			1	95	503	88	1	11
			4	99	131	78	2	20
			24	100	22	58	0	42
Recycling 2			1	83	486	86	3	11
			4	100	146	85	1	14
			24	100	25	64	0	36
Recycling 3			1	45	319	81	9	10
			4	77	80	82	6	12
			24	96	13	70	1	29
Recycling 4			1	14	162	78	14	8
			4	54	40	78	10	12
			24	93	7	84	1	14

a: the catalyst has been treated with H_2 (20 bar) in isopropanol at 70°C for 4h before introducing cinnamaldehyde in the reactor.

b : the catalyst has been treated with H_2 (20 bar) in isopropanol at 70°C for 4h before introducing cinnamaldehyde in the reactor and the catalyst amount has been divided by two.

The use of a support is essential to access to high performances and good recyclability (by dispersing the nanoparticles and preventing their agglomeration) [10]. It has been shown recently that it can promote one path over other giving a specific product and then affecting the selectivity of a catalytic reaction [50, 51]. Few layer graphene has been chosen as support since

its 2D morphology allows high accessibility of reactants [52-54], and graphitic supports have been theoretically shown to favor C=O adsorption on Pt and subsequent preferential hydrogenation [31]. In the case of cinnamaldehyde hydrogenation, graphene in comparison with other kind of carbonaceous support has shown an enhanced selectivity for the production of cinnamyl alcohol [52, 55]. We have thus decided to support our CCs on FLG, and more precisely to grow them directly on the support. We have recently grown cobalt nanowires on metallic foams and on a silica alumina support by modification of a wet chemistry approach, which produces free nanowires in solution. We have shown that when a support is present, in order to reproduced the same shape as in the absence of a support, it is necessary to increase the amount of the ligands [56, 57]. The fact that in the presence of the support in the reaction medium that allow producing shape controlled nano-objects fails to reproduce the same shape of nanocrystals indicates that part of the ligand is adsorbed on the support and is not available any more for directing the nanocrystal growth. We have thus employed the same strategy for the growth of the CCs on the FLG support. It has to be noted that the ratio Pt/ODA is important for controlling nanocrystal morphology. Thus, increasing the ODA concentration to reach a Pt/ODA mass ratio of 1/100 allows the selective growth of supported concave nanocubes (SCCs) on the FLG support. In Fig.2a-b we present the TEM images of the as-obtained supported nanocrystals of two different sizes SCC-8 and SCC-50 (7.8 ± 3.0 nm and 50.2 ± 13.8 nm, respectively). The 8 nm CCs are not all of them very well-defined and homogeneous, and we can discern the presence of small classical non-concave nanocubes among the CCs (Fig. 2a). The 50 nm CCs grown on the FLG are well-shaped (Fig. 2b). Both catalysts have comparable ligand content (Pt/L ~ 2), higher than in the case of both CC-11 and CC-45. Both catalysts have been used for the cinnamaldehyde hydrogenation, employing the same reaction conditions as for the free nanocrystals. The SCC-50 catalyst was evaluated at 4 h also. In Fig.

2c and 2d we present the results on their catalytic performances (See also Table 2 entries 5 and 6, respectively).

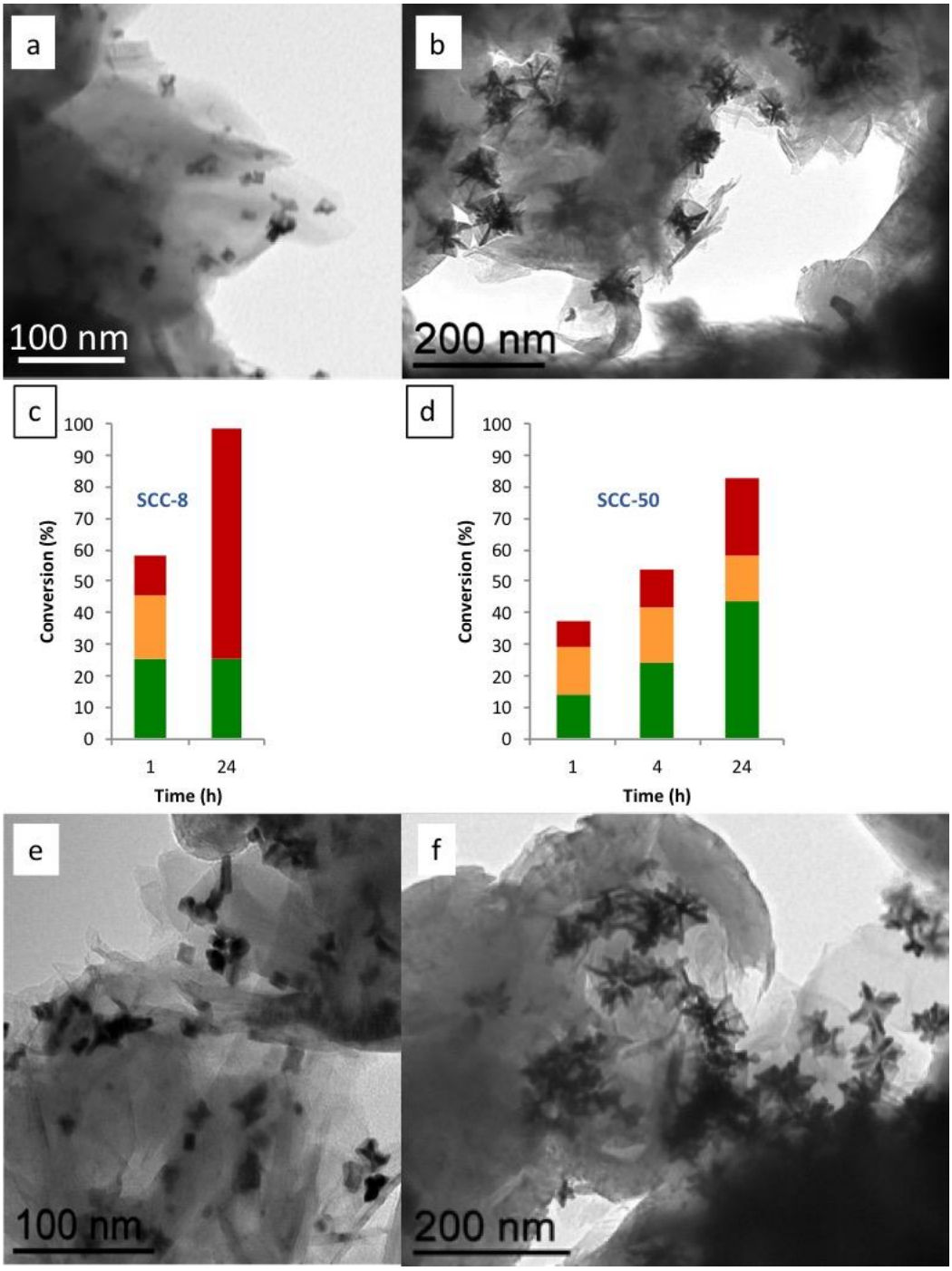

Fig. 2. FLG-supported Pt CCs. (a) TEM images of the as-prepared SCC-8 (b) SCC-50; catalytic results (c) SCC-8 and (d) SCC-50; TEM after 24h reaction of (e) SCC-8 and (f) SCC-50 catalysts.

In Fig. 2e and 2f we present the TEM images of the two spent catalysts after 24h reaction, which show that in both cases aggregation has been avoided thanks to the immobilization of the nanocrystals on the support. Concerning their shape evolution after 24 h catalytic reaction, for SCC-8 there is not a marked modification of the general sample aspect; however, the fact that the SS-8 are less well defined does not allow safe conclusions. The impact of the hydrogenation reaction for SCC-50 is small as in the case of the CC-45.

The activity of the SCC-8 is higher than the one of SCC-50 both at 1 and 24 h. This is due to the smaller nanocrystal size. Since no aggregation has taken place during the reaction at 24 h we have complete conversion for the SCC-8 catalyst, in contrast to the non-supported CC-11. We notice that initially the SCC-8 and SCC-50 selectivity for COL are very similar (43 and 38 %, respectively). This is an interesting result because these two catalysts have the same exposed facets and similar Pt/L molar ratio (Pt/L ~ 2), but very different particle size. Therefore, it seems that the particle size is not the most important factor to control the selectivity. If we correlate this result to the one obtained by comparing the NCC-6 and CC-45, we can propose a significant influence of the type of facets on COL selectivity. Thus, it seems that the concave facets favor COL formation. On SCC-8, complete hydrogenation after 24h produces HCOL as the major product. The SCC-50 shows the same tendency as CC-11 and CC-45, favoring the selectivity towards COL as the reaction time is increased. The selectivity evolution indicates a preferential hydrogenation of the HCAL over hydrogenation of the COL.

The difference in catalyst characteristics (supported or not, different size, shape, ligand content) makes a straightforward comparison of their performances complicated. This is clearly shown in Fig. S2 in which the plots of activity at 1 hour versus size and versus ligand content of our catalysts do not allow to suggest any simple correlation of activity to size or ligand content. Similarly, the selectivity to COL does not seem to directly correlate with size (Fig. S2). Nevertheless, COL selectivity can be well correlated to the Pt/L ratio in CC and SCC samples.

Indeed, Fig. 3a. shows that the higher the ligand content, the better the COL selectivity. Concerning the activity, a very good correlation, shown in the plot of Fig. 3b can be found when we consider a more complex parameter integrating both size and ligand content. Thus, activity is increased either by decreasing nanoparticle size and/or the ligand content. On these figures, the red squares, which correspond to the NCC-6 catalyst performances do not fit in any of these plots. This means that these correlations hold only when we consider similar facets. Finally, from Fig. 3c we can safely conclude that both activity and selectivity to COL are improved when the CCs are immobilized on FLG.

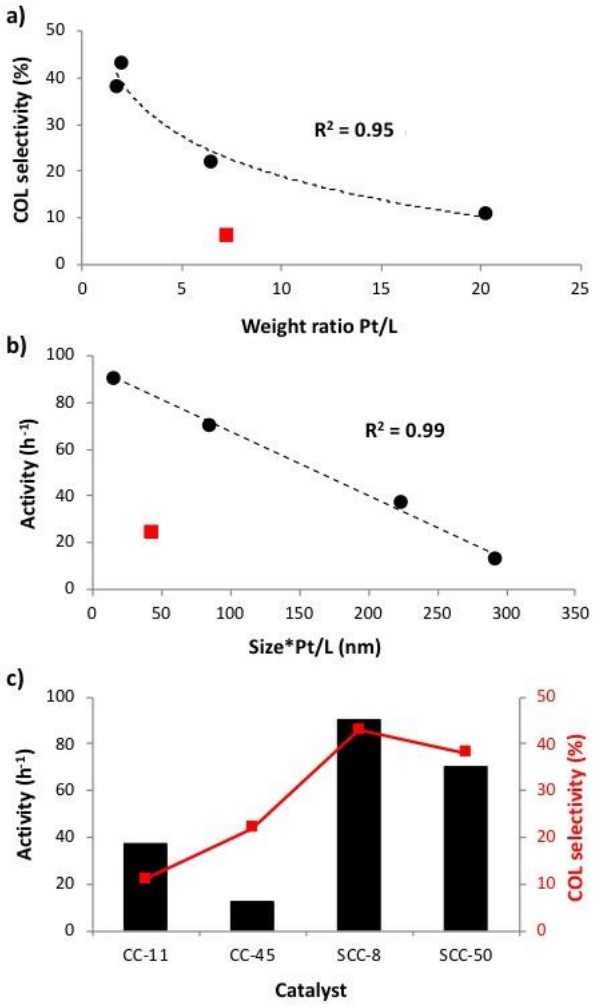

Fig. 3. Plots of (a) catalyst selectivity towards COL versus Pt/L weight ratio; (b) catalyst activity versus (size*Pt/L) The 1 h reaction activity and selectivity were considered. The red

squares correspond to the results obtained with NCC-6. (c) activity (h^{-1}) and COL selectivity at 1h of catalysis plotted for each CC and SCC catalysts.

The shape homogeneity and resistance under hydrogenation conditions of the SCC-50 and the possibility to isolate and recycle it has incited us to test the recyclability of this catalyst. For these recycling experiments, we have slightly modified the reaction conditions. While the preparation of the catalysts has been performed in the glove-box, the catalysts have been stocked under ambient conditions. We have thus performed a pre-reduction step during 4 hours under the same reaction conditions as during the catalytic runs, the only difference being the absence of cinnamaldehyde. This treatment, first tested on the CC-45 catalyst, was found: (i) not to impact the Pt morphology, (ii) despite its slight agglomeration, to marginally improve the activity, probably due to the more reduced state of the surface, and (iii) to substantially improve the selectivity towards COL. (Table 2, entry 3 and Fig. S3). This effect is probably associated to an even greater surface crowding upon pre-saturation by H_2. This interpretation was suggested by Durndell *et al*. who observed an improvement of the selectivity to COL upon H_2 pressure increase [24]. For the recycling of the SCC-50 we have decided to perform this pre-reduction step. In order to better monitor the conversion at 24h, in addition to the pre-reduction step, we have decreased by half the amount of catalyst used, designated as SCC-50-H_2. In Fig. 4 we present the TEM micrograph of the catalyst after H_2 pre-reduction (Fig. 4a), the results of the catalytic tests (Fig. 4b-f) (see also Table 2 entry 7), as well as the TEM image of the spent catalyst after the end of all recycling experiments (Fig. 4g).

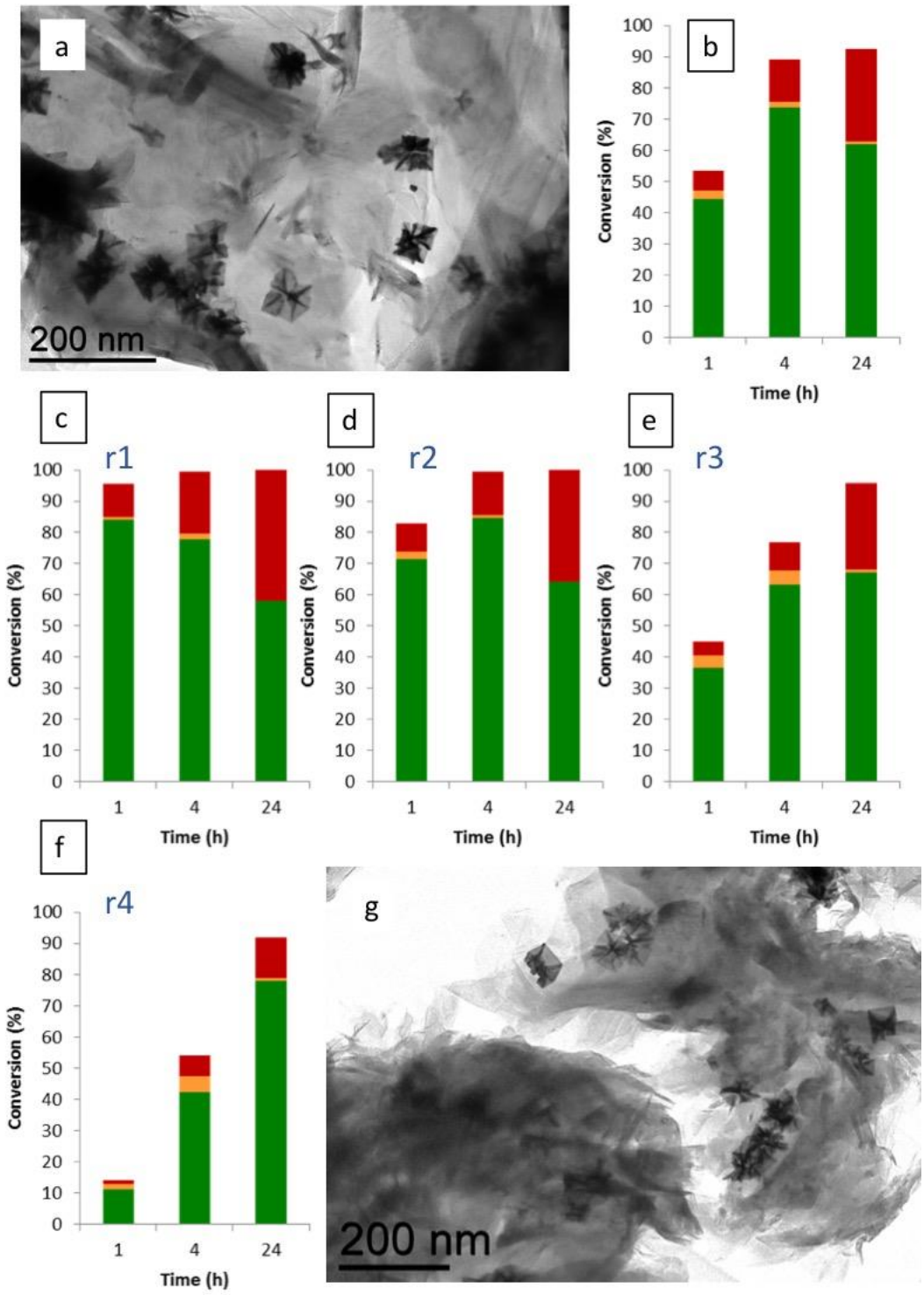

Fig. 4. (a) TEM image of the as-prepared SCC-50-H_2 catalyst and (b) its catalytic performance; (c)-(f) catalytic performances of four successive recycling tests; (g) TEM image of the SCC-50-H_2 catalyst after the last recycling.

From our data, we see that both activity and selectivity to COL are improved for SCC-50-H_2 as compared to SCC-50. Indeed, and despite the lower catalyst amount, the conversion is almost complete after 4 hours with a very good selectivity towards COL, which, as expected, is further hydrogenated to HCOL upon longer reaction time. The counterintuitive increased activity upon dilution can be explained if we consider that by reducing the catalyst amount, the ligand concentration in solution is also reduced, which could favor higher activities, albeit without penalizing the good selectivity to COL. The same tendencies are observed after two successive recycling steps, however, while selectivity to COL continues to be high, the activity drops in the third and fourth recycling steps. Since no major morphological alterations are obvious from the TEM images of the spent catalyst, we believe that the apparent deactivation is a result of loss of catalyst during its washing after each recycling step. On the other hand, the high selectivity to COL, which is practically the same until the end, indicates that the catalyst surface remains always sufficiently covered by ligands. Considering the fact that the catalyst is washed at the end of each run, and that the catalyst concentration is divided by two, this result seems somehow contradictory to our findings that high ligand content favors COL selectivity. It is then likely that despite the fact that the amount of ligand is diminished with time, the ligand distribution between Pt and FLG could vary throughout the reaction. Thus, the FLG could act as a ligand reservoir that guarantees a minimum ligand associated to the nanoparticles re-establishing the equilibrium between FLG- and Pt-associated ligands. Thus, ligand content is found within an optimal range, which guarantees adsorption modes that favor C=O hydrogenation. This parameter of ligand distribution between the active phase and the support merits to be further studied as it is very likely also important for other reactions and with several supports and metal catalysts. “Ligand-M” interaction versus “Support-Ligand” interaction could then be tuned in order to optimize the catalytic performances.

A direct comparison with other catalytic systems, most of them without organic ligands is not straightforward, however, the SCC-50-H_2 catalyst presents comparable results to the ones of some of the best Pt catalysts reported in the literature (Fig. S4, Table S1). It is worth noting that the activity was calculated over the total Pt amount. Thus, if we compare the activity of the SCC-50-H_2 catalyst (500 h^{-1}) with the best activities found in the literature: 3%Pt/C (size: 1.6 nm, activity:1300 h^{-1}) [58] and 3.6 Pt/FLG (size: 2 nm; activity: 1600 h^{-1}) [59] and if we consider the difference in Pt nanoparticle size, the TOF of SCC-50-H_2 should be much higher. We believe that this is due to the presence of high index facets.

4. Conclusions

Unprecedent Pt concave nanocubes presenting {110} facets have been directly grown on FLG support *via* an *in-situ* process based on a wet chemistry approach. Non-supported and supported CCs of similar size have been tested as catalysts for the selective hydrogenation of cinnamaldehyde. Despite the fact that it is a real challenge to isolate the effect of each parameter (morphology, ligands, support) on the catalytic performances of these systems in cinnamaldehyde hydrogenation, several conclusions can be drawn. First, the use of few layer graphene as support allowed a stabilization of the CCs. The supported catalysts show better selectivity towards COL and better activity than the free CCs. This is mainly due to CC size and Pt/L ratio and not to a direct influence (metal-support interaction) of the support. The COL selectivity is well correlated to the Pt/L ratio for SCC and CC catalysts. An influence of the type of facets exposed is also proposed, {110} facets leading to higher selectivity as compared to {100} facets. The activity of the catalysts is well correlated to size. Pt/L for the concave nanocubes (supported or not). There also, we propose an influence of the facets exposed; the {110} facets leading to higher activity particularly compared to literature results with conventional Pt catalysts. However, the facet-reactivity correlation is not ligand-independent,

and it is not impossible that the role of ligands is facet dependent. The ligands are an important actor that allows reactivity modulation through interaction not only with the surface of the metal but also with the support. A good understanding of the performances of ligand-containing supported catalysts is very challenging due to the fact that such systems are defined by more parameters than non-supported nanocatalysts or supported catalysts that do not contain ligands. These parameters cannot be easily dissociated. Further studies should be undertaken in order to: (i) determine the ligand distribution between the metal and the support, (ii) optimize the ligand amount, and (iii) study the effect of different ligands and different supports. We finally believe that despite these inherent difficulties, in order to fully exploit the potential of wet chemistry approaches, ligands in supported catalysts should be regarded as an additional opportunity, through which catalytic performances can be finally finely tuned, just as in homogeneous catalysis.

Acknowledgements

L.P. thanks the University of Toulouse for financial support, D. Y. thanks the ANR for financing the DENSAR project (ANR-14-CE07-0025- 01).

References

[1] K. An, G. A. Somorjai, ChemCatChem, 4 (2012) 1512-1524.

[2] AT. Bell Science, 299 (2003) 1688-1691.

[3] R. Jin, Nanotechnol Rev. 1 (2012) 31-56.

[4] L. M. Rossi, J. L. Fiorio, M. A. S. Garcia, Camila P. Ferraza, Dalton Trans. 47 (2018) 5889-5915.

[5] S. Campisi, M. Schiavoni, C. E. Chan-Thaw, A. Villa, Catalysts 6 (2016) 185.

[6] W. Huang, Q. Hua, T. Cau, Catal. Lett. 144 (2014) 1355-1369.

[7] M. J.-L. Tschan, O. Diebolt, P. W. N. M. van Leeuwen, Top. Catal. 57 (2014) 1054-1065.

[8] L. Jin. B. Liu. S. Duay. J. He. Catalysts 7 (2017) 44.

[9] I. Geukens, D.E. De Vos., in Nanomaterials in Catalysis, Wiley-VCH Verlag GmbH & Co. KGaA, 2013, pp. 311-330.

[10] N. J .S. Costa, L. M. Rossi, Nanoscale, 4 (2012) 5826-5834.

[11] P. Munnik, P. E. de Jongh, K. P. de Jong, Chem. Rev. 115 (2015) 6687-6718.

[12] R.M. Rioux, H. Song, M. Grass, S. Habas, K. Niesz, J.D. Hoefelmeyer, P. Yang, G.A. Somorjai, Top. Catal. 39 (2006) 167-174.

[13] P. Tan, G. Li, R. Fang, L. Chen, R. Luque, Y. Li, ACS Catal. 7 (2017) 2948-2955.

[14] C. Zhang, S. N. Oliaee, S. Y. Hwang, X. Kong, Z. Peng, Nano Lett. 16 (2016) 164-169.

[15] Y. Lu, Y. Jiangab and W. Chen, Nanoscale 6 (2014) 3309-3315.

[16] F. Zaera, Chem. Soc. Rev. 42 (2013) 2746-2762.

[17] S. Nishimura, K. Ebitani, ChemCatChem 8 (2016) 2303-2316.

[18] Y. Wu, D. Wang, Y. Li, Chem. Soc Rev. 43 (2014) 2112-2124.

[19] F. Behafarid, B. Roldan Cuenya, Top Catal. 56 (2013) 1542-1559.

[20] F. Zaera, ACS Catal. 7 (2017) 4947-4967.

[21] I. Lee, F. Delbecq, R. Morales, M. A. Albiter, F. Zaera, Nature. Mater. 8 (2009) 132-138.

[22] Y. Zhu, F. Zaera, Cat. Sci. Tech. 4 (2014) 955-962.

[23] A. J. Plomp, H. Vuori, A. O. I. Krause, K. P. de Jong, J. H. Bitter, Appl. Catal. A 351 (2008) 9-15.

[24] L. J. Durndell, C. M. A. Parlett, N. S. Hondow, M. A. Isaacs, K. Wilson, A. F. Lee, Sci. Rep. 5 (2015) 9425.

[25] W. O. Oduro, N. Cailuo, K. M. K. Yu, H. Yangy, S. C. Tsang, Phys. Chem. Chem. Phys. 13 (2011) 2590-2602.

[26] X. Qi, M. R. Axet, K. Philippot, P. Lecante, P. Serp, Dalton Trans. 43 (2014) 9283-9295.

[27] Y. Gu Y. Zhao, P. Wu, B. Yang, N. Yang, Y. Zhu, Nanoscale 8 (2016) 10896-10901.

[28] Z. Jiang, Y. Zhao, L. Kong, Z. Liu, Y. Zhu, Y. Sun, ChemPlusChem 79 (2014) 1258-1262.

[29] B. Wu, H. Huang, J. Yang, N. Zheng, G. Fu, Angew. Chem. Int. Ed. 51 (2012) 3440-3443.

[30] I. Cano, A. M. Chapman, A. Urakawa, P. W. N. M. van Leeuwen, J. Am. Chem. Soc. 136 (2014) 2520-2528.

[31] F. Delbecq, P. Sautet, J. Catal. 152 (1995) 217-236.

[32] J.C. Serrano-Ruiz, A. López-Cudero, J. Solla-Gullón, A. Sepúlveda-Escribano, A. Aldaz, F. Rodríguez-Reinoso, J. Catal, 253 (2008) 159-166.

[33] W. Zang, G. Li, L. Wangab, X. Zhang, Catal. Sci. Technol. 5 (2015) 2532-2553.

[34] K. Zhou, Y. Li, Angew. Chem. Int. Ed. 51 (2012) 602-613.

[35] S. K. Vatti, K. K. Ramaswamy, V. Balasubramanaian, J. Adv. Nanomat. 2 (2017) 127-132.

[36] H. J. Kim, B. Ruqia, M. S. Kang, S. B. Lim, R. Choi, K. M.Nam , W. S.Seo, G. Lee, S.-I. Choi, Sci Bull, 62 (2017) 943-949.

[37] G. Collins, M. Schmidt, C. O'Dwyer, G. McGlacken, J. D. Holmes, ACS Catal. 4 (2014) 3105-3111.

[38] Z. Zhang, J. Hui, Z. Liu, X. Zhang, J. Zhuang, X.Wang, Langmuir 28 (2012) 14845-14848.

[39] L. Zhang, H. Su, M. Sun, Y. Wang, W. Wu, T. Yu, J. Zeng Nano Res. 8 (2015) 2415-2430.

[40] M. Jin, H. Zhang, Z. Xie, Y. Xia, Angew. Chem. Int. Ed. 50 (2011) 7850-7854.

[41] Q. Chen, Y. Yang, Z. Cao, Q. Kuang, G. Du, Y. Jiang, Z. Xie and L. Zheng, Angew. Chem. Int. Ed. 55 (2016) 9021-9025.

[42] Z. Quan, Y. Wang, J. Fang, Acc. Chem. Res. 46 (2013) 191-202.

[43] J. Zhang, Q. Kuang, Y. Jiang and Z. Xie, NanoToday 11 (2016) 661-677.

[44] 1 C.M. Pradier,T. Birchem, Y. Berthier, G. Cordier, Catal. Lett. 29 (1994) 371-378.

[45] R. Bacsa, I. Cameán, A. Ramos, A. B. Garcia, V. Tishkova, W. S. Bacsa, J. R. Gallagher, J. T. Miller, H. Navas, V. Jourdaine, M. Girleanu, O. Ersen, P. Serp, Carbon 89 (2015) 350-360.

[46] L. Peres, D. Yi, S. Bustos-Rodriguez, C.Marcelot, A.Pierrot, P.-F. Fazzini, I. Florea, R. Arenal, L.-M. Lacroix, B. Warot-Fonrose, T. Blon, K. Soulantica submitted to Nanoscale.

[47] K. B. Vu, K. V. Bukhryakov, D. H. Anjum, V. O. Rodionov, ACS Catal. 5 (2015) 2529-2533.

[48] I. Schrader, J. Warneke, J. Bachenköhler, S. Kunz, J. Am. Chem. Soc. 137 (2015) 905-912.

[49] P. Mäki-Arvela. J. Hajek. T. Salmi. D. Y. Murzin. Appl. Catal. A. 292 (2005) 1-49.

[50] W. Oberhauser, C. Evangelisti, R.P.Jumde, R. Psaro, F. Vizza, M. Bevilacqua, J. Filippi, B. F. Machado, P. Serp, J. Catal. 325 (2015) 111-117.

[51] H. Wang, K. An, A. Sapi, F. Liu, G. A. Somorjai, Catal. Lett. 144 (2014) 1930-1938.

[52] Z. Sun, Z. Rong, Y. Wang, Y. Xia, W. Du, Y. Wang, RSC Adv. 4 (2014) 1874-1878.

[53] Z. Rong, Z. Sun, Y. Wang, J. Lv, Y. Wang, Catal. Lett. 144 (2014) 980-986.

[54] J. Shi, R. Nie, P. Chen, Z. Hou, Catal. Commun. 41 (2013) 101-105.

[55] X. Ji, X. Niu, B. Li, Q. Han, F. Yuan, F. Zaera, Y. Zhu, H. Fu, ChemCatChem 6 (2014) 3246-3253.

[56] J. Harmel. A. Berliet. K. Dembélé. C. Marcelot. A.-S. Gay. O. Ersen. S. Maury. A. Fécant. B. Chaudret. P. Serp. K. Soulantica. ChemCatChem 10 (2018) 1614-1619.

[57] J. Harmel, L. Peres, M. Estrader, A. Berliet, S. Maury, A. Fécant, B. Chaudret, P. Serp, K. Soulantica, Angew. Chem. Int. Ed. 57 (2018) 10579-10583.

[58] D. Hu, W. Fan, Z. Liu, L. Li, ChemCatChem 10 (2018) 779-788.

[59] J. Shi, R. Nie, P. Chen, Z. Hou, Catal.Commun. 41 (2013) 101-105.